Supporting information

Effect of HNO_3 functionalization on large scale graphene for enhanced tri-iodide reduction in dye-sensitized solar cells

Santanu Das,[a‡] P. Sudhagar,[b‡] Eisuke Ito,[c] Dong-yoon Lee,[d] S.Nagarajan,[b] Sang Yun Lee,[c] Yong Soo Kang,[b*] and Wonbong Choi [ab*]

[a]Department of Mechanical and Materials Engineering, Florida International University, Miami, Florida, 33174, Fax: (+1)305-348-1932, E-mail: choiw@fiu.edu.
[b]WCU Program Department of Energy Engineering, Hanyang University, Seoul 133791, South Korea, E-Mail: kangys@hanyang.ac.kr.
[c]Flucto-Order Functions Research Team, RIKEN-ASI, Saitama 351-0198, Japan.
Corresponding authors: choiw@fiu.edu (WC); kangys@hanyang.ac.kr (YSK)

Section S1: Surface morphology analysis

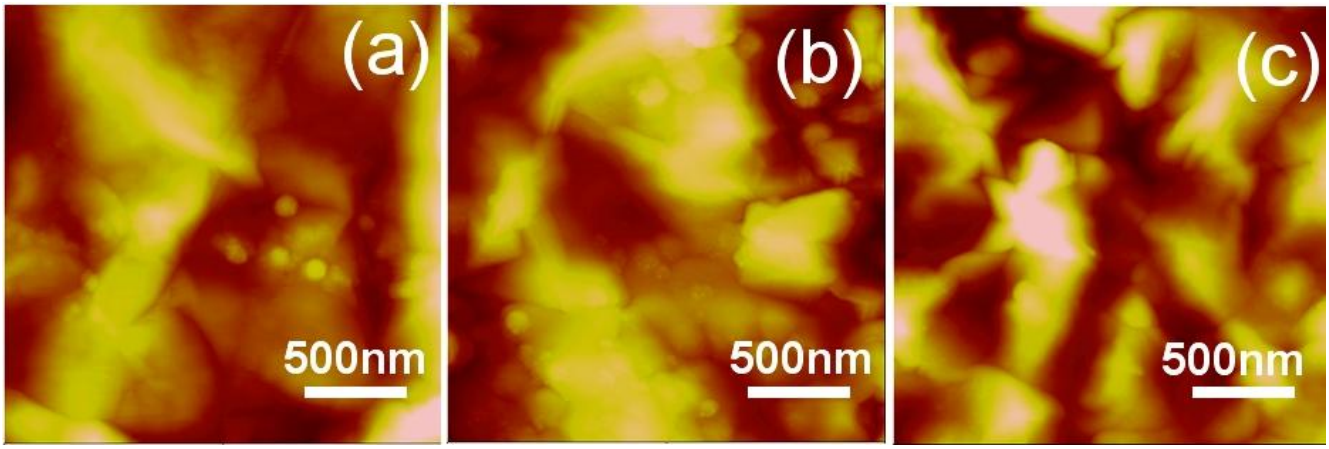

Fig. S1: AFM images of (a) PG (b) 20HDG and (c) 70HDG electrodes.

The surface topography of graphene on FTO (Ted Pella Inc.) was investigated using AFM (NanoScope IIIa, Veeco Instruments Inc., USA). The Non-contact/Tapping Mode AFM probes were purchased from NanoWorld AG (NANOSENSORS^{TM}, Switzerland) which had relatively stiff cantilevers with a high spring constant (30.0–59.0 N/m). Figure S1 a, b and c represents the surface morphology of pristine graphene, 20HDG and 70 HDG respectively. From the AFM analysis we found that there was no major change in surface morphology or surface structure observed even after the HNO_3 treatment of graphene.

Section S2: X-Ray Photoelectron Spectroscopy

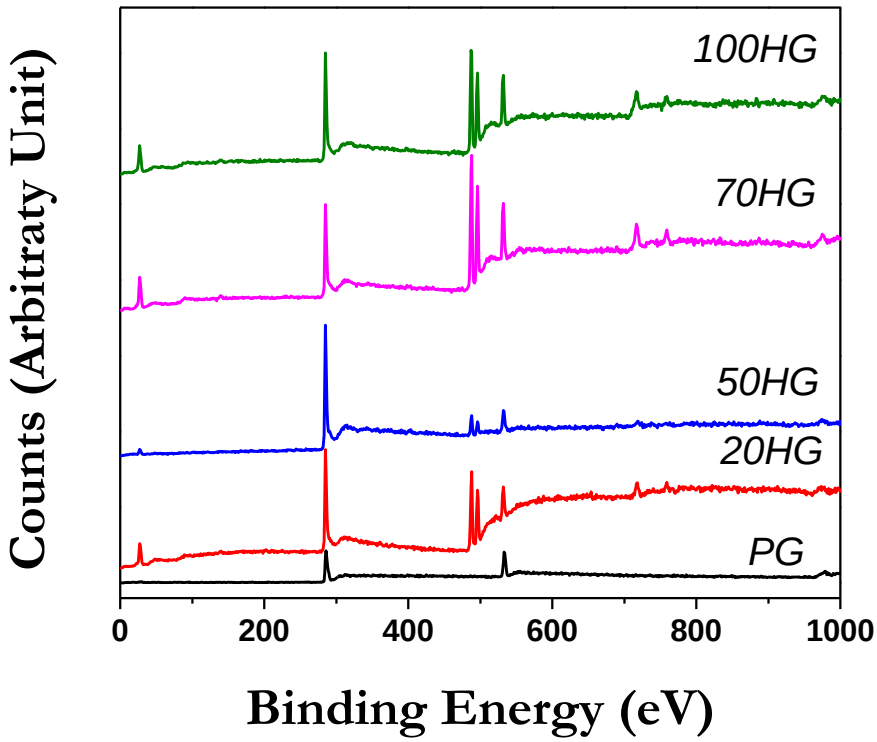

Fig. S2: Illustrate comparison X-ray photoelectron spectra of pristine graphene and acid doped graphene electrodes.

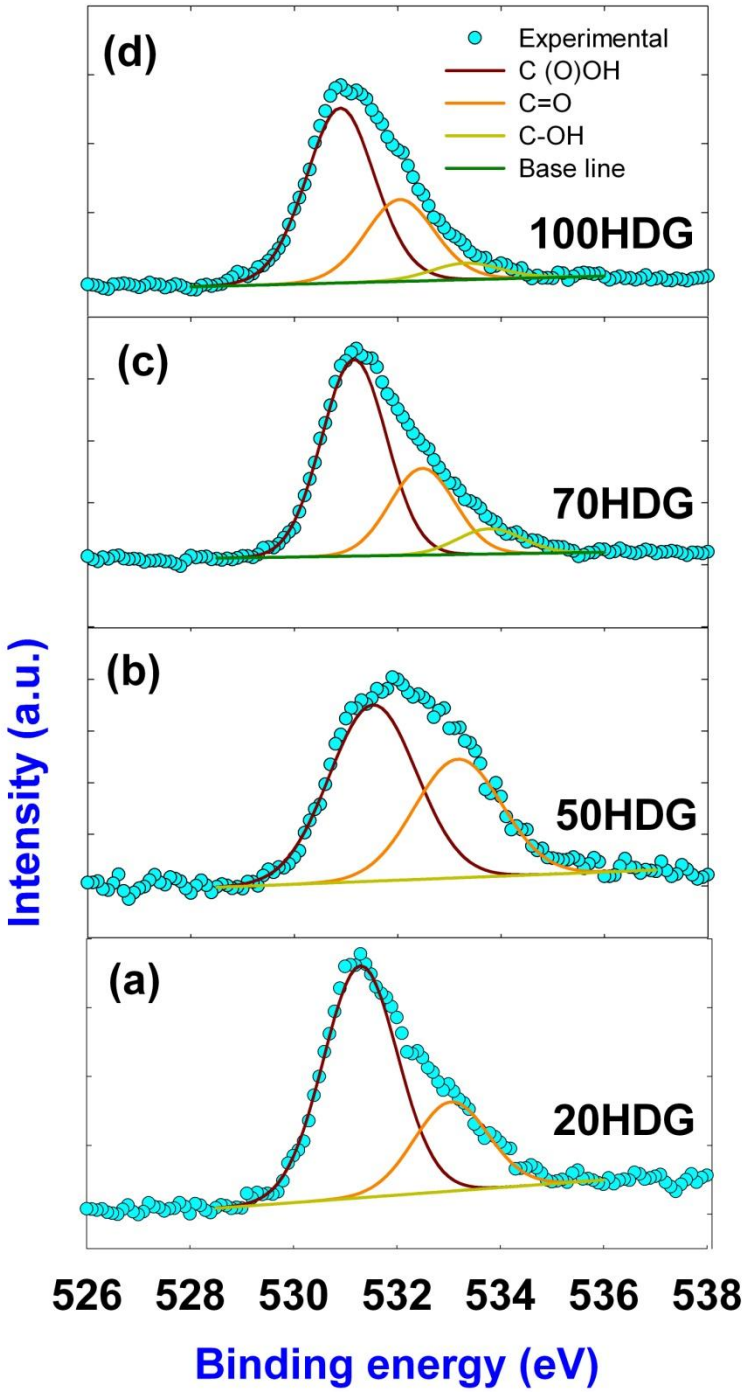

Fig. S3: De-convoluted X-ray photoelectron spectra of oxygen peaks represent different stretching modes of C-O covalent bonds for (a) 20% HNO_3 treated (b) 50% HNO_3 treated (c) 70% HNO_3 treated and (d) 100% HNO_3 treated graphene.

Section S3: Electrochemical Characterizations

The decrease in charge transfer resistance is attributed to the increase in exchange current density J_0 at the electrode-electrolyte interface as shown in the Figure S4 (b). The exchange current density was calculated using the following equation S1:

$$J_0 = \frac{RT}{nFR_{ct}} \quad \text{(S1)}$$

Where, R_{ct} is the charge transfer resistance calculated from the EIS spectra, R is the universal gas constant, T is the temperature in K, n = number of electrons contributing to the charge transfer at the interface and F is the Faraday's constant.

Exchange current density is the kinetic component which arises due to the charge transfer from the counter electrode to the I^{3-} ions at the counter electrode-electrolyte interface. The temperature dependent charge transfer resistance exchange current density curves for different graphene counter electrodes are illustrated in Figure S4 (b) which follows the Arrhenius equation as per the equation S2.

$$J_0 = I_0 e^{(-\frac{Ea}{RT})} \quad \text{(S2)}$$

Where, E_a is the Activation Energy; R is the Universal gas constant; I_0 is the exchange current density at T = infinity; and T is the Temperature in K.

Figure S4 b, illustrates the exchange current density of the symmetric cell with the temperature for different un-doped and doped graphene electrodes. We found that, the exchange current density increases with increasing doping concentrations (enhancement of C-O bonds which attributed to the protonation in the graphene as described in the XPS section of the main

manuscript) which is support the enhancement of improved electro catalytic activity of the graphene counter electrodes owing to its Fermi level shift.

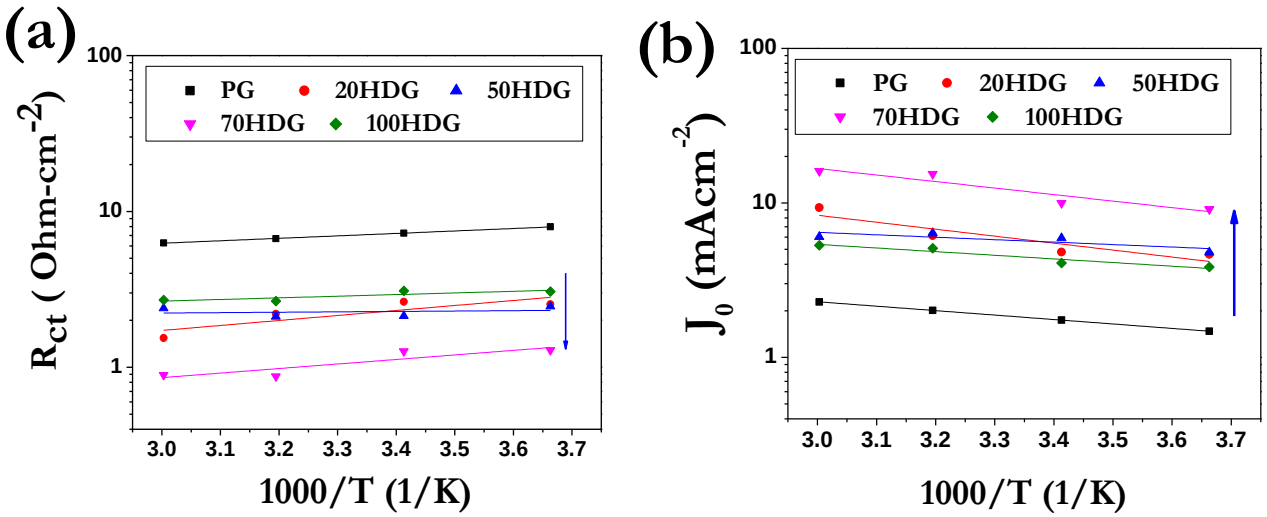

Fig. S4: (a) Charge transfer resistance vs. temperature and (b) exchange current density vs. temperature plot for graphene and different concentration of acid doped graphenes represent the stability of different counter electrodes at temperature from 273K to 333K.

Section S4: Fourier Transform Infrared Spectroscopy (FTIR)

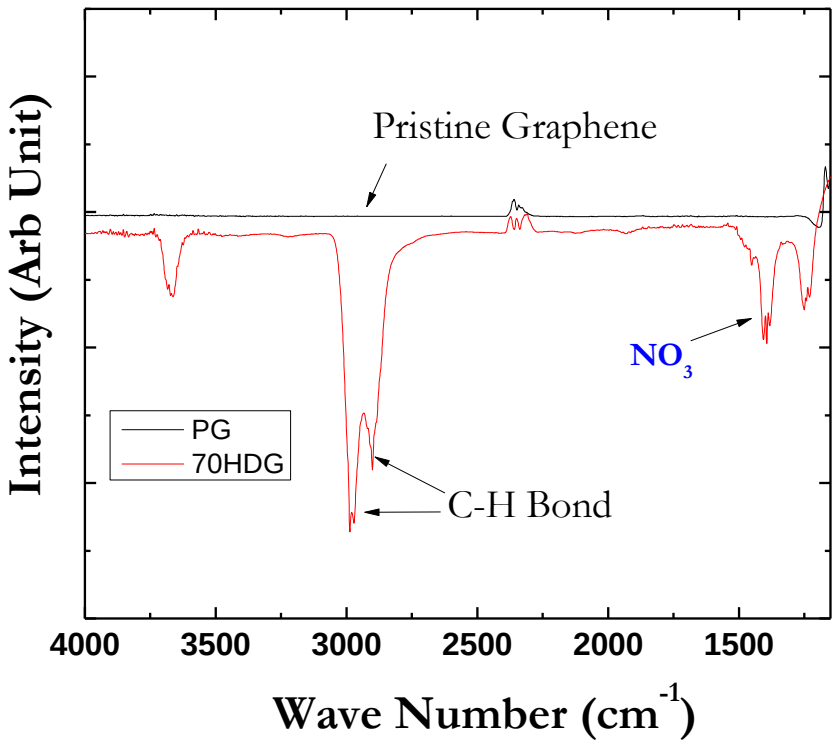

Fig. S5: Comparison FTIR spectra of Pristine and 70% HNO_3 doped graphene (70HDG) which shows the formation of C-NO_3 and C-H stretching bond in HNO_3 doped graphene.

Section S5: Full Cell Characteristics

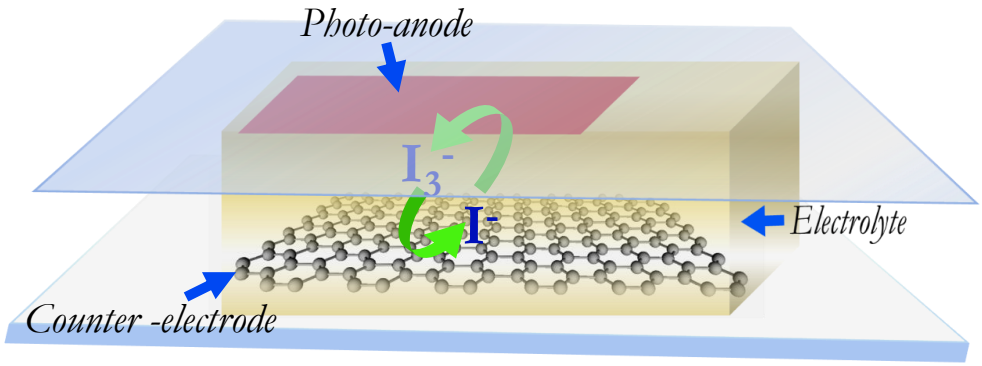

Fig. S6: Schematic illustrates the dye sensitized solar cells based on different doped and undoped graphene counter electrodes.

Section S6: Optical Characterizations:

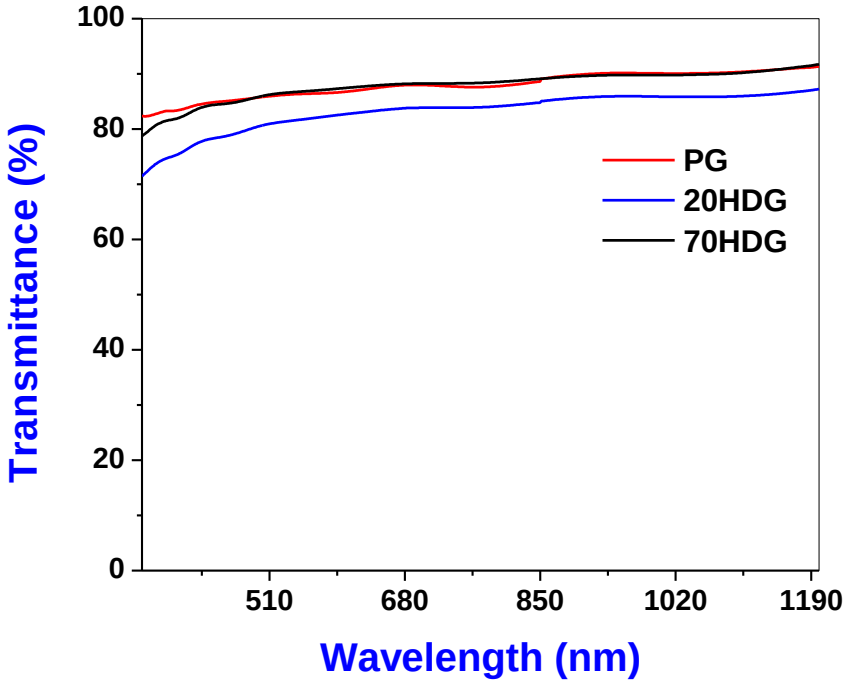

Fig. S7: Illustrates comparison optical transmittance spectra of pristine and nitric acid treated graphene electrodes. Note that graphene electrodes showing ~ 85% transmittance at visible region.